International Journal of Engineering Education (IJEE)
e-ISSN : 2540-9808

Intelligent Control of Switched Reluctance Motor Using Fuzzy Logic and SMC Controller for EV Applications

Vijayalakshmi K[1]*, Srinivas Kn[1]
[1]SRM IST, India
e-mail: vijik.rk@gmail.com

Abstract - *Switched Reluctance Motors have expanded their field of application in recent years, from a control system stepping motor to high torque e-vehicle applications. High-speed operation and a light-weight driving motor are critical elements for an effective electric vehicle design. SRM's low torque-to-weight ratio and magnetless rotor design make it ideal for use in electric vehicles with less weight and low cost. The only limitation with switched reluctance motors is torque ripple and vibrations. There have been a variety of techniques to reducing torque pulsations in the SRM, by which vibration and noise can be reduced. In this paper, an optimization technique is used in switching controllers in and a comparison is done between a sliding mode controller (SMC) with a modified reaching law and by using Fuzzy Logic Controller (FLC). By using matlab Simulink the magnitude of torque ripple is simulated and compared for 8/6 pole SRM. The results shows that the torque ripple is reduced in fuzzy compared to SMC significantly.*

Keywords *– electric vehicle, fuzzy controller, switched reluctance motor, sliding mode control, torque ripple.*
Submission: September 4, 2022 Correction: December 12, 2022 Accepted: December 12, 2022

Doi: http://dx.doi.org/10.14710/ijee.4.2.42-57
[How to cite this article: Vijayalakshmi K, Srinivas Kn. (2022). Intelligent Control of Switched Reluctance Motor Using Fuzzy Logic and SMC Controller for EV Applications. *International Journal of Engineering Education, 4(2)*, 42-57. doi: http://dx.doi.org/10.14710/ijee.4.2.42-57]

1. Introduction

Due to the requirement for frequent brush replacement, brushed and commutator-based machines have fallen out of favour. Though BLDC Motors provide simple control, the larger torque ripple during commutations [1] and inferior torque performance of PMSM are the key disadvantages when compared to BLDC Motors. PMSM allows for precise torque and speed control. However, PMSM Motors have several significant drawbacks, including: Magnetic Deterioration of Permanent Magnets at High Temperatures and High Speeds [2], Motor construction necessitates rare-earth materials, which are scarce and have environmental consequences [3], and High Speed Operation is limited due to the presence of permanent magnets in the rotor, which has poor mechanical strength.Switched Reluctance Motors, on the other hand, are becoming more popular and ideal for EV applications, as they offer more benefits than PMSM and BLDC. The design is simplified by the winding and magnet-less rotor construction, which also eliminates the shortcomings of PMSM. It's a machine with a low moment of inertia and a high torque-to-weight ratio. For improved torque and speed performance, all existing direct torque control and vector control algorithms demonstrated for IM control can be adapted to SRM.Due to unipolar nature of stator current injected only during rising inductance interval for supplying necessary motoring torque results in discontinuous input current and thereby high input THD and Low power factor. [2] Proposes a midpoint converter topology based on CuK- Sepic dual output converters for power factor correction during discontinuous inductor current operation especially at lower speeds. The voltage following methodology employed in converter brings down the input line current THD. Another disadvantage in SRM drives is, the large vibration and acoustic noise due to changing radial forces between stator and rotor during commutation interval [3].The SRM Drives, are doubly salient drives, having saliency in both the stator and rotor, resulting in non-linearity in magnetic flux couplings. SRM Drives' non-linear nature becomes more obvious at higher speeds, making excitation/demagnetization control non-uniform and difficult across a large speed range. Due to this, there is very high torque ripples in SRM drives. There are currently three methods for reducing torque ripple in SRM drives, one of which is machine design. Due to variances in aligned and unaligned inductances, a lower number of phases in SRM Motor architecture results in larger torque ripple[4]. As a result, multiphase SRM or a large number of stator poles are preferable. A magnetic equivalent circuit (MEC) technique is proposed in [5] for simulating the magnetic flux and torque performance of rotor segmented axial field SRMs. The MEC

approach to machine modelling and design can simulate machine performance over a wide range of operating ranges and load torque circumstances in order to understand flux linkage changes and propose a machine design solution for the torque pulsations issue in SRM. The second technique is to use novel topologies of power electronic converters [6]. When compared to other converters such as the C-dump circuit and the N+1 Power electronic converter, the asymmetric half bridge converter topology is the most preferred since it provides independent phase control and has lower torque pulsations. The third method is to use controller design, TSF (Torque Sharing Function), DTC (Direct Torque Management), DITC (Direct Torque Control) for independent torque and speed control as well as superior dynamic torque performances [7]. In order to reduce torque pulsations in SRM drives, fuzzy controllers, sliding mode controllers, model adaptive predictive control, neural and genetic algorithm based controllers are used. The Direct Torque Control algorithm used in SRM Motors [8] to reduce torque ripple uses higher current in non-effective rotor positions while simultaneously limiting MTPA (Maximum torque per ampere). Furthermore, the challenge of SRM Motor control at low and high speeds necessitates two distinct techniques. Late magnetization reduces torque at high speeds, while late demagnetization results in a negative torque value. The research proposes ideal start and stop times, as well as periods of excitation and de-excitation, based on the actual motor speed, supply voltage, and current restrictions. Traditional PI Controllers are ineffective in controlling non-linear control systems, hence they are not recommended for SRM Drives [9]. [10] Proposes a switching variable proportional desaturation PI regulator, which eliminates integral saturation difficulties in PI regulators and provides higher dynamic performance as well as speed control stability across all stages of operation. However, the inherent flaws caused by mathematical models, as well as dynamic performance stability at higher operation speeds and torque ripple pulsations, must be investigated. When used with the DTC Strategy, [11] proposes a sliding mode controller (SMC) with a new reaching law to effectively reduce speed deviations in SRM Motors, as well as an anti-disturbance sliding mode observer (AD-SMO) for significant reductions in torque ripple, which is high especially at higher speeds due to high non-linearity in the Flux and rotation angle relationship. However, the suggested SMC and AD-SMO did not take into account the issue of thermal management restrictions in converter circuits, particularly at higher speeds, and the optimization necessary in control aspects. The use of a cost function instead of a Hysteresis function to the selection of voltage vectors in the targeted sector of SRM Operation during excitation and demagnetization periods for a reference torque and optimizing the selection for needed flux linkage. Model predictive control algorithm can control the flux linkage in advance, and the torque ripple performance is superior than DTC.

2. Selection of SRM Motor Configuration and Power Electronic Converter Topology of SRM Drives

SRM is based on the motion of variable reluctance. The stator poles are wound, and the rotor has a laminated iron core with no winding. When the stator phase winding is switched to supply or energized. The rotor is drawn to the stator by the magnetic field formed in the stator, and the rotor orients itself to the stator in the minimum reluctance position.

When rotor rotates from unaligned to aligned position there is inductance variation (dL/dθ). In this paper, an SRM motor with 8 stator poles and 6 rotor poles (8/6 SRM) as shown in figure 1 is considered for modeling and simulation. It shows that each phase consists of four poles that are simultaneously excited by an external DC power source, which forces the pole from unaligned position θu to aligned position θa

The Co- Energy curve is shown in figure 2. The resultant torque produced in SRM can be given by equation.

Stored Magnetic Energy = $\frac{1}{2}Li^2$

T = $\partial E / \partial \theta$ |i = constant

T = $\frac{1}{2}i^2\frac{dL}{d\theta}$

As the rotor rotates from its unaligned to its aligned positions, the inductances change. The direction of current has no effect on torque creation because current is squared. The fluctuation or slope of inductance should, nevertheless, be positive when producing motoring torque. Thus, only during the positive inductance slope period is current is injected for phase excitation.

The step angle or Stroke = $\boldsymbol{\varepsilon}$= $\frac{2\pi}{qNr}$ = 7.5'

Where q is No of Phases = 8 & Nr is number of rotor poles = 6

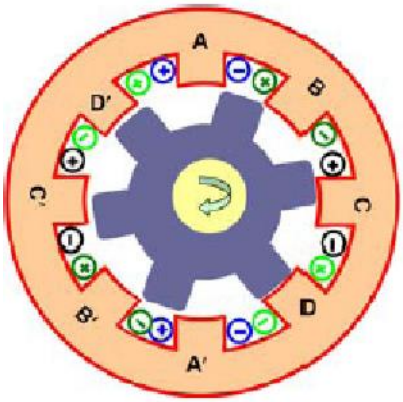

Figure 1. Construction of 8/6 SRM

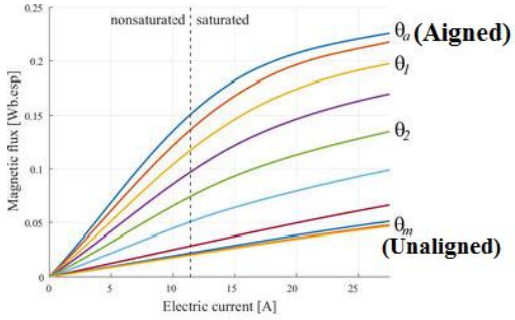

Figure 2. Inductance waveform showing aligned and unaligned variations

The most common converter topology for switched reluctance motor drive is the asymmetric half bridge converter shown in Figure 3. Two IGBT switches and two diodes are used in each phase circuit. The converter topology for 8/6 SRM has a total of 8 IGBT switches and 8 Diodes.

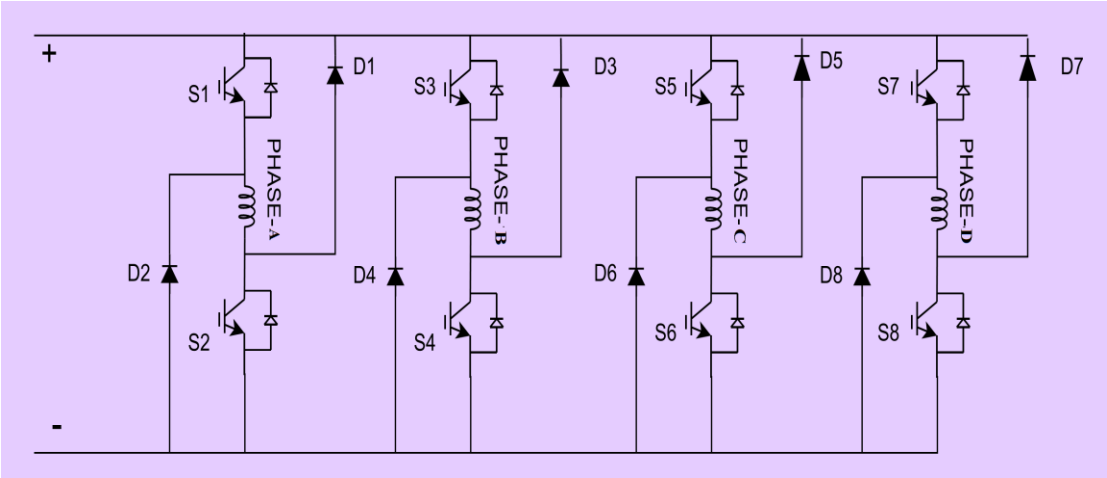

Figure 3. Asymmetric Half Bridge Converter circuit diagram

The asymmetric half bridge converter has excellent fault tolerance as well as superior torque performance [12]. During motoring or magnetization mode, both the S1 and S2 devices are turned on, and a DC voltage is applied to the winding. When S2 is switched off, the winding current freewheels through S1 and D1 in freewheel mode, and demagnetization of the winding occurs through D1 and D2 when both the IGBTs S1 and S2 are turned off. The modes are represented graphically in figure 4.

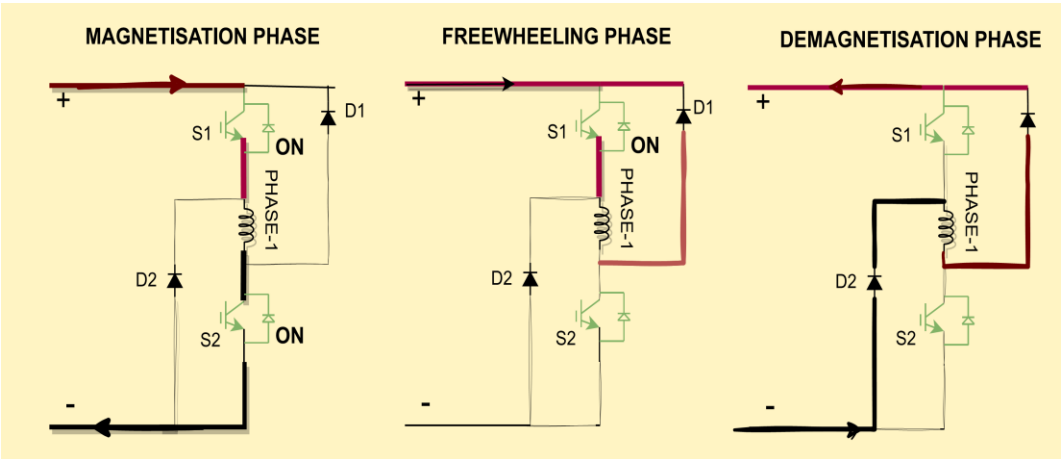

Figure 4. Operating modes of SRM with AHB Converter

The Converter topology selected in this paper is Asymmetric half bridge converter. The converter circuit is shown in figure 5. In this asymmetric bridge type is followed with free-wheeling diode and the capacitor. The signal to the gate circuit will be given from the fuzzy logic controller and the SMC controller.

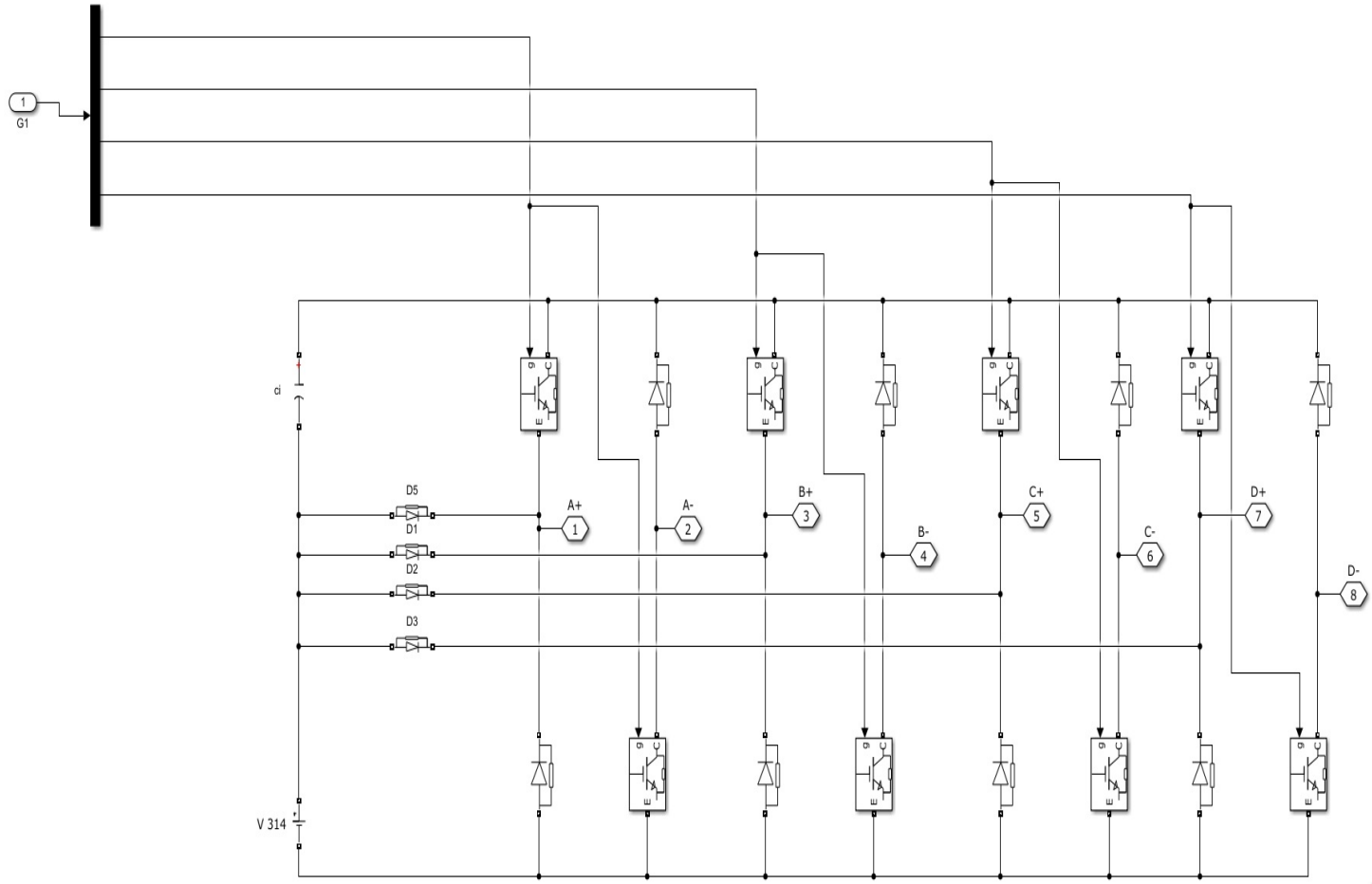

Figure 5. Converter topology for 8/6 pole SRM

2.1 Mathematical Modeling of SRM

The geometry and torque generating mechanism of SRMs are unique, providing significant issues in machine modeling. The air gap fluctuates greatly due to the dual saliency in both the stator and the rotor, meaning that the machine flux linkage is a nonlinear function of rotor position. SRMs operate in a magnetic saturation region as well. This makes machine modeling and control more difficult.

The torque equation of a motor and load can be expressed as , $\mathbf{T_e(i,\theta) = T_L + B\omega + J\frac{d\omega}{dt}}$

The Electrical torque of SRM motor as derived above,

$\mathbf{T_e(i,\theta) = \frac{1}{2} i^2 \frac{dL}{d\theta}}$

Because SRM is non-linear, a simplified model is usually used. As a result, ignoring the mutual inductances between the phases results in a simplified equivalent circuit is shown in figure 6.

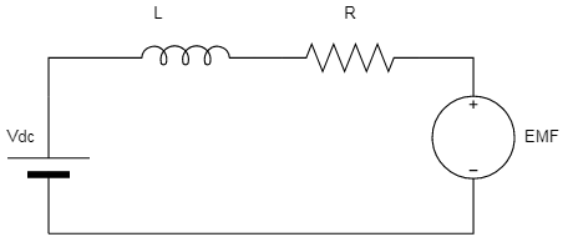

Figure 6. Equivalent Circuit of SRM

The Voltage Equation can be given as,

$\mathbf{V = ir + L(i,\theta)\frac{\partial i}{\partial t} + i\frac{\partial L(i,\theta)}{d\theta}\omega}$

The Rotational component is back emf, $\mathbf{e = i\frac{\partial L(i,\theta)}{d\theta}\omega}$

Back emf is a linear function of rotational speed, $\mathbf{e \propto \omega}$

The EMF is induced in the phase windings as the motor rotates. The resultant emf generated opposes the applied excitation voltage to the phase windings and as a result, rate of change of phase current is limited. Hence the rotational back emf is very important concept to understand the phase current dynamics in SRM. Ignoring the effects of resistance, the equation can be expressed as,

As the EMF is a linear function of rotor speed as expressed by equation. The rate of change of current depends mainly on the speed of the motor.

$$\frac{(V-e)}{L} = \frac{di}{dt}$$

Where V = voltage in Volts, I = Current in A, L = inductance in H, ω = angular velocity

The induced voltage does not limit the rate of change of current at low speeds. As a result, the high current will cause large winding copper losses and also considering the thermal limit, the reference current chopping control is adapted this ensure safe working within thermal limits and also torque production that sufficiently meets the torque command.

The conduction angle is the difference between the Turn-on (**θ**on**)** and Turn-off angles (**θ**off**)**. The selection of the optimal conduction angle is critical in achieving the desired torque performance and torque quality [13]. At low speeds, torque is achieved by using PWM of the DC voltage to control the current rise; however, at higher speeds, the current rise is largely controlled by back EMF, and thus torque performance is largely dependent on the conduction angle. The longer the conduction period as a result of the delayed turn off angle, the more negative torque is produced. The torque and current waveform is shown in figure 7.

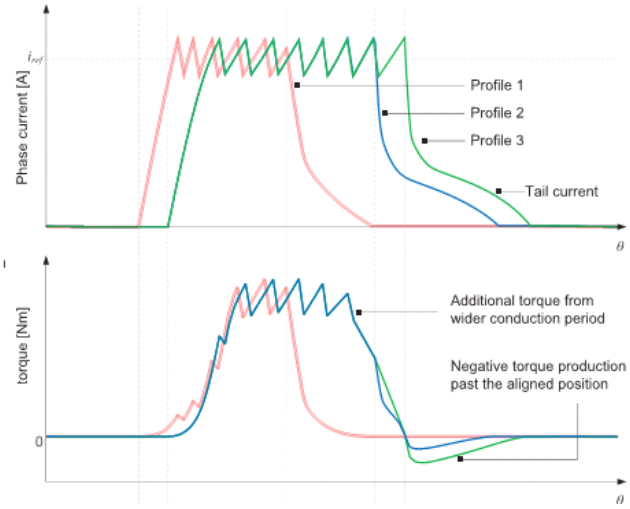

Figure 7. Torque and Phase current waveforms of SRM [13]

The Torque to current conversion equation shall be expressed as,

$$T_e(i, \theta) = \frac{1}{2} i^2 \frac{dL}{d\theta}$$

$$i = \sqrt{[2\, T_k(i, \theta) \;/\; L_k]}$$

Where $L_k = \frac{\partial L(i,\theta)}{d\theta}$

2.2 Block Diagram of The Control System

The control system of a switched reluctance motor is based on mathematical modeling. There are two control loops: the outer speed control loop and the inner current controller loop. The motor speed is obtained from the encoder mounted in the switched reluctance motor, and the speed encoder signal (velocity) is translated to rotor position by the discrete time integrator block. The speed controller compares the reference speed to the speed feedback obtained from the encoder, and the error is processed by the controller block, which is a sliding mode controller or controller, and the output of the controller will set the torque reference. The Block diagram is shown in Fig. 8.

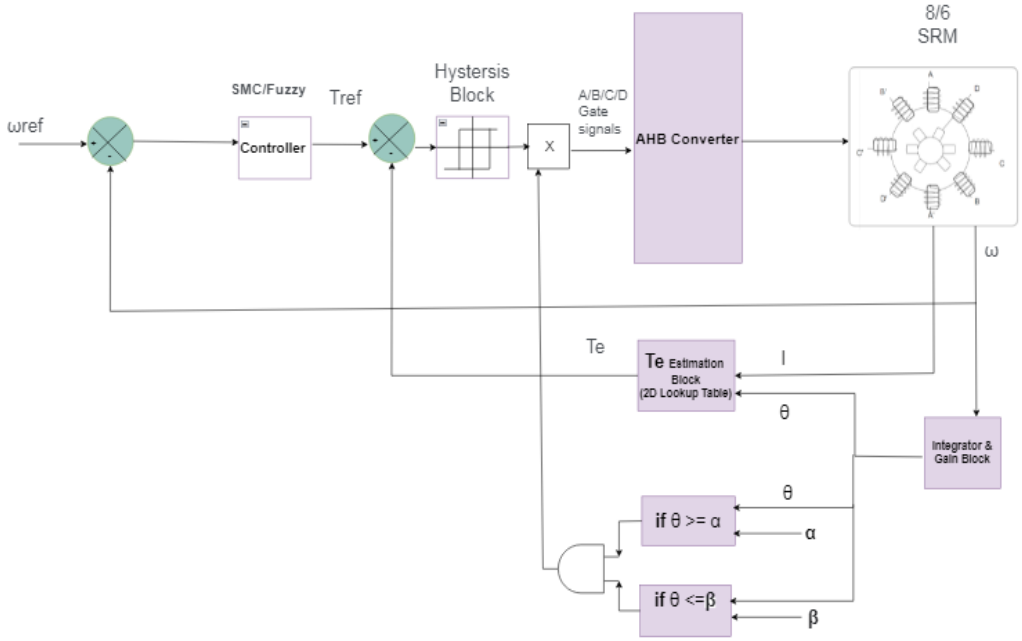

Figure 8. Block diagram of 8/6 pole SRM with fuzzy and SMC

The actual torque is calculated using a two-dimensional lookup table is shown in figure 9, that expresses torque as a function of excitation current and rotor position.

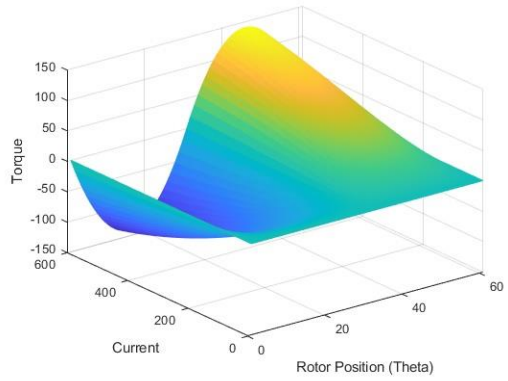

Figure 9. Estimated torque surface viewer w.r.t to current and Rotor position (Theta)

The controller's reference torque is compared to the estimated torque and the resultant current is processed by the current hysteresis block. The position of the rotor is compared to alpha (turn on angle) and beta (turn off angle). The pulses are sent to IGBT devices in the AHB Converter only when the rotor position is within the switching angle period.

The peak current at low speeds must be controlled to be at some commanded value i_{ref} in order to prevent the current from exceeding the thermal limits and to keep the machine running smoothly. A hysteresis band is represented by I_{up} and I_{lo} as shown in Fig.10. The tolerance of the hysteresis band can be expressed as μ.

$I_{up} = I_{ref} \times (1 + \mu)$

$I_{lu} = I_{ref} \times (1 - \mu)$

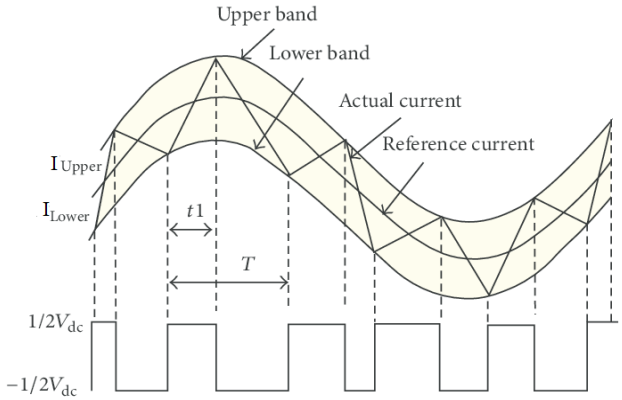

Figure 10. Hysteresis Controller

The switching frequency of the hysteresis current controller is determined by the phase inductance and the width of the hysteresis band at any given time. As a result, SRM's control system runs at a variable switching frequency. Fundamentally, if the rate of change of current is higher at a given instant, the current will diverge from the hysteresis band more quickly, causing the current controller to respond by switching the device faster. On the other side, a slower rate of current change indicates that switching will take longer.

3. Design of Proposed Sliding Mode Controller

Sliding mode control is one of the Robust Control strategies for bringing a control system to a stable equilibrium point. SMC control has a sliding plane where the equilibrium point is located. The system's controlled trajectory is far away from the plane, and a series of control

actions added to the system will bring it to the sliding plane or sliding surface, regardless of its initial conditions. The trajectory will glide along the plane until it reaches the equilibrium point O when it reaches the plane.

(A) Governing Mathematical Equations

The Governing differential equations of a switched reluctance motor is as follows,

$$\frac{d\theta}{dt} = \omega \quad (1)$$

$$\frac{d\omega}{dt} = \frac{1}{J}(T_e - T_L - B\omega) \quad (2)$$

As the motor torque is the function of rotor position angle and current, the equation could be elaborated as,

$$\frac{d\omega}{dt} = \frac{1}{J}(_{j=1}\sum T_e^j(\theta_j, i_j) - T_L - B\omega) \quad (3)$$

Where ω is angular speed, T_L is load torque, B is viscous fraction coefficient and J is the inertia constant respectively.

Considering, $x_1 = \omega$ and $x_2 = \frac{d\omega}{dt}$

$$x_2 = \frac{1}{J}(_{j=1}\sum T_e^j(\theta_j, i_j) - T_L - Bx_1)$$

The first derivative of x_2 can be represented as,

$$\dot{x}2 = \frac{1}{J}(\dot{T}_e - Bx_2)$$

$e_{x1} = x_1 - x_{1d}$

Where $e_{x1}$is the speed error expressed as difference of measured (x1) and reference speed (x_{1d}).

The phase variable state equation can be simplified asper the (LTI) continuous-time system, $\dot{x} = Ax + Bu$

$$\begin{bmatrix} \dot{e}_{x1} \\ \dot{e}_{x2} \end{bmatrix} = \begin{bmatrix} 0 & -1 \\ 0 & -a \end{bmatrix} \begin{bmatrix} e_{x1} \\ e_{x2} \end{bmatrix} + \begin{bmatrix} 0 \\ b \end{bmatrix} U \quad (4)$$

Where, $a = \frac{B}{J}$ $b = \frac{1}{J\tau}$

U is the control output of SMC Controller. After the effect of integrator, it is the total reference torque of SRM.

(A) Sliding surface:

Now, let us assume that there exist sliding mode control law *U* which forces the phase trajectory to slide on the hyperplane *S* on a phase plane for *c*>0, λ∈*R* given by,

$S(x, t) = (Ce_{x1} + e_{x2})$

U is a control signal that, regardless of drive system parameter alterations, is utilized to govern the speed error dynamics. The following is a description of the sliding line:

$$S = c(\omega - \omega_{ref}) + \frac{d(\omega - \omega ref)}{dt}$$

Where *c*is a constant greater than 0.

$\dot{S} = C\dot{e}_{x1} + \dot{e}_{x2}$

To maintain on a sliding surface, S=0;

$Ce_{x1} = -e_{x2}$

$Ce_{x1} = -\dot{e}_{x1}$

$\dot{e}_{x1} = -Ce_{x1}$

$e_{x1}(t) = e^{-ct}e_{x1}(0)$ or $\omega = \omega_{ref}(1 - e^{-ct})$

Thus after reaching the sliding mode of system, Speed is only related with the parameters c.

As long as c > 0, then the $\lim_{t\to\infty} \omega = \omega_{ref}$, System is stable. If c values are higher, the response is faster.

In order to verify the stability of the reaching law, the Lyapunov function $V = s^2/2$ is chosen.

The key point in designing a sliding mode controller is to find a control strategy for the plant input U (t) such that, $\frac{dV(s)}{dt} < 0$, This condition should be regardless of the spatial position of the system state

To satisfy the existence condition of the sliding-mode speed controller, the following must be satisfied:

$$\lim_{S\to 0} s\frac{ds}{dt} <= 0 \quad (5)$$

The control law U (t) is designed to meet the above condition.

if we employ the control strategy, then the system state will be dragged towards the stable hyperplane S(x, t) = (c e +ė)

The system state will reach the hyperplane surface in finite time. Once it reaches the surface then it slides along the surface towards the equilibrium point.

$$u(t) = \begin{cases} U^+ & \text{if } S(\mathbf{x}, t) > \Delta \\ U^- & \text{if } S(\mathbf{x}, t) < -\Delta \\ \text{Previous state} & \text{Otherwise} \end{cases}$$

Where Δ is an arbitrarily small value or the hysteresis band The introduction of a hysteresis band with the boundary conditions $S = \Delta$ and $S = -\Delta$ provides a form of hysteresis control without control chattering.

The MATLAB Simulink model of SMC controller for 8/6 pole SRM is shown in figure 11. The speed encoder feedback signal and current feedback is obtained for closed loop control.

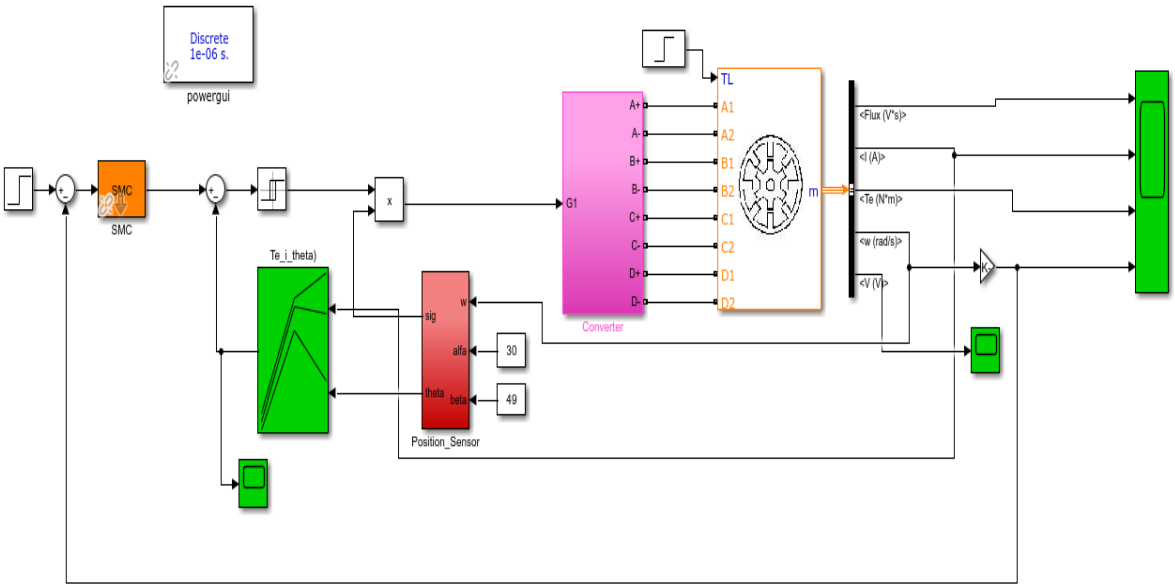

Figure 11. SRM control with siding mode controller

The speed is converted to Rotor position angle through position estimator block is shown in figure 12.

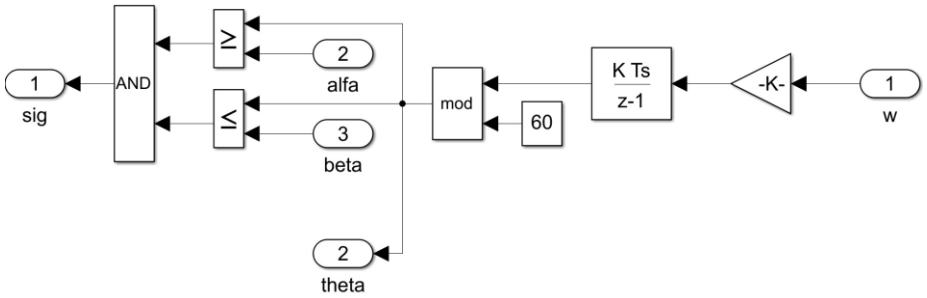

Figure 12. Position sensor block

The sliding mode controller is developed for the switching function (s) and control function U(t) as shown in Fig.13.

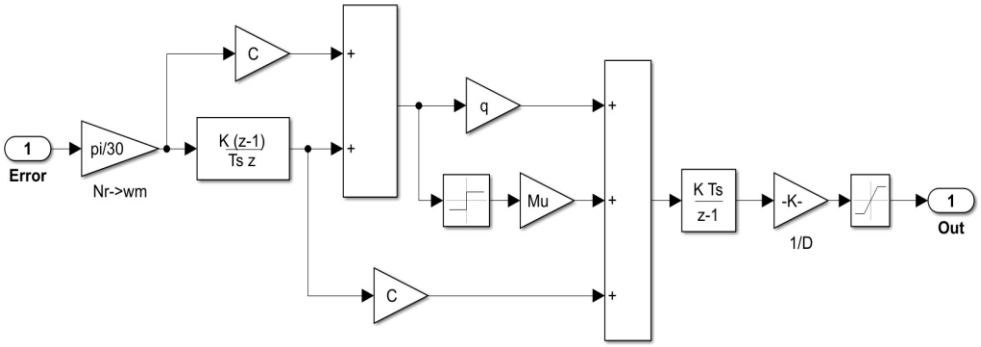

Figure 13. Sliding Mode Controller Simulink Model

4. Fuzzy Logic Controller

4.1 Fuzzy Logic Control

Real-life circumstances can be extremely complicated. The fundamental advantage of fuzzy logic controllers is their ability to incorporate experience, logical reasoning, intuition, and heuristics into the system rather than relying on mathematical models. The characteristic function of the classical set assigns a value of 1 or 0 (Binary set) to each individual in the universal set, therefore distinguishing between members and non-members of the crisp set in question. A fuzzy set is a collection of components with different degrees of set membership. In fuzzy set theory, many types of membership functions are often employed for fuzzification of the inputs. By mapping each element to a membership value between 0 and 1, the membership function for a set uniquely describes that set. The membership function is chosen based on previous experience and the problem's specificity. The block diagram of fuzzy logic controller block is shown in 14.

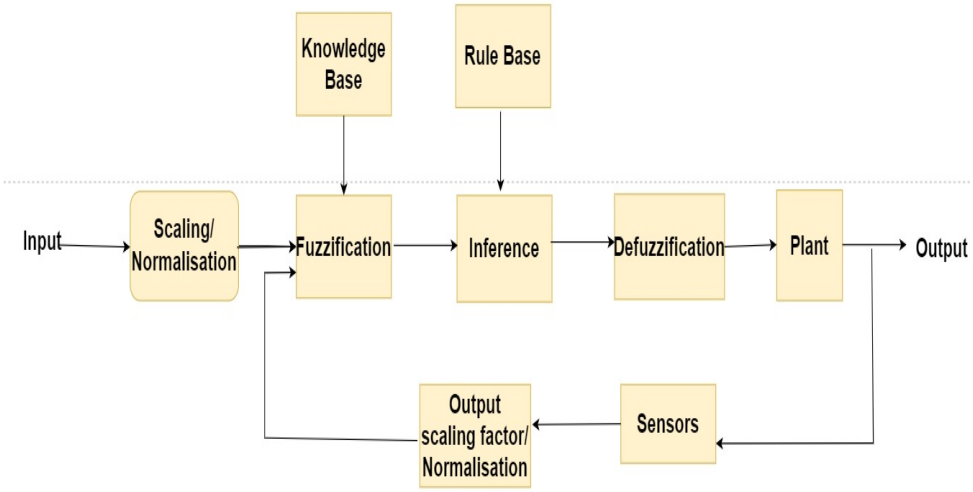

Figure 14. Block diagram of fuzzy controller

Prior to transforming crisp sets to fuzzy sets, the inputs are scaled and normalized. Fuzzification is the process of converting crisp values to fuzzy values. The conversion of fuzzy values is represented by membership functions. Membership function is designated as μ.

4.2 Design of Proposed Fuzzy Logic Controller

The MATLAB Simulink model for Fuzzy logic Control of 8/6 SRM drive is shown in figure 15. The speed encoder feedback signal and current feedback is obtained for closed loop control.

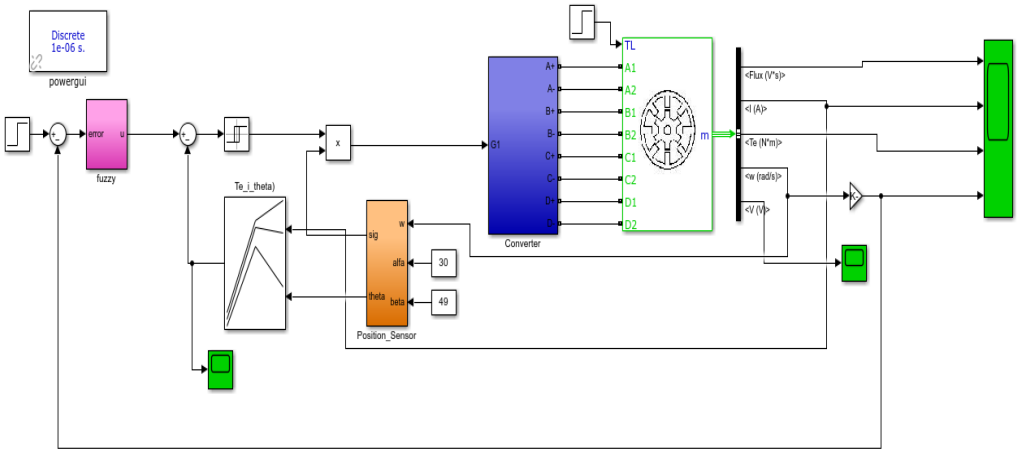

Figure 15. SRM control with fuzzy logic controller

The speed error (ω – ω_{ref}) represented by E and Error change $\frac{d(\omega - \omega ref)}{dt}$represented by EC are the crisp inputs to the fuzzy controller system and the output defuzzified crisp output is multiplied by a proportional gain to generate the control output. The fuzzy controller block is shown in figure 16.

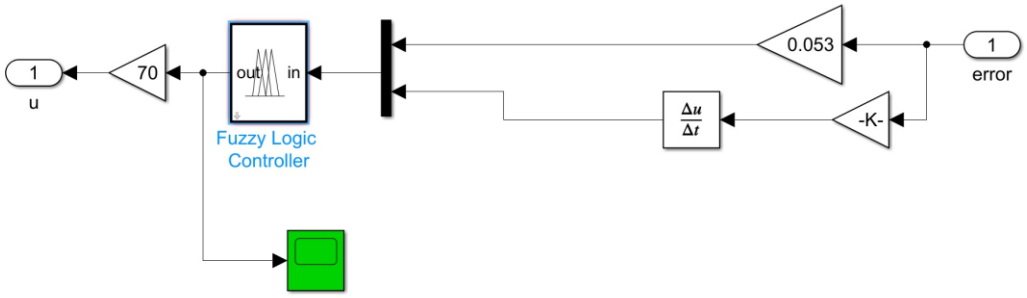

Figure 16. Fuzzy controller simulink model

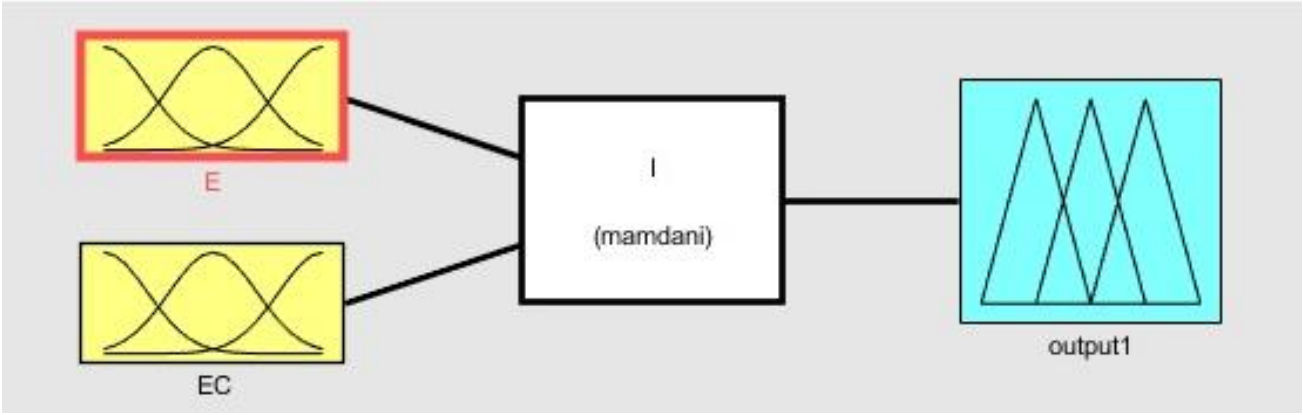

Figure 17. Fuzzy input-output membership functions

The fuzzy membership function is shown in figure 17. The fuzzy inference engine is a process that uses if-then rules and fuzzy mechanisms to link input fuzzy sets to output fuzzy sets in order to get a reasonable result from fuzzy inputs. The Mamdani type and the Sugeno type are two forms of fuzzy inference systems. The Mamdani model is used in this simulation. Mamdani fuzzy systems use rule base for fuzzy input sets for determining the output distribution. The design of fuzzy controller system is as follows,

1. Determining a set of fuzzy rules

The inputs and output are all divided into five fuzzy subsets: [NB,NM, NS, ZE, PS, PM,PB], where NB, NM, NS, ZE, PS, PM and PB mean negative big, negative medium, negative small, zero, positive small, positive medium and positive big, respectively.

2. Fuzzifying the inputs using the input membership functions

The membership functions of the inputs and output are triangular and Z & S-shaped at the ends. The minimum value is used for operation (AND), and the centroid method is used for defuzzification.

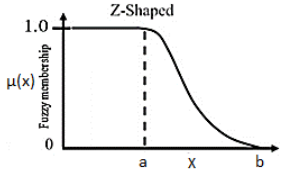

Z-Membership function:

$$\mu(x; a, b) = \begin{cases} 1, & x \le a \\ 1 - 2\left(\frac{x-a}{b-a}\right)^2, & a \le x \le \frac{a+b}{2} \\ 2\left(\frac{x-b}{b-a}\right)^2, & \frac{a+b}{2} \le x \le b \\ 0 & x \ge b \end{cases}$$

S-Membership function:

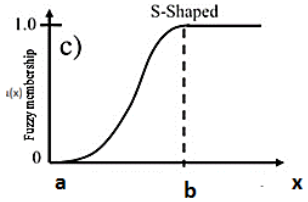

$$\mu(x; a, b) = \begin{cases} 0, & x \le a \\ 2\left(\frac{x-b}{b-a}\right)^2, & a \le x \le \frac{a+b}{2} \\ 1 - 2\left(\frac{x-a}{b-a}\right)^2, & \frac{a+b}{2} \le x \le b \\ 1 & x \ge b \end{cases}$$

3. Combining the fuzzified inputs according to the fuzzy rules to establish rule strength. The rules consist of 49 IF-THEN rules. The E is the error and EC is the rate of the error change. The fuzzy rules are tabulated in Table 1.

Table 1. Fuzzy Rules

Parameters		ERROR CHANGE (EC)						
		NB	NM	NS	ZE	PS	PM	PB
ERROR (E)	NB	NB	NB	NB	NB	Z	Z	PS
	NM	NB	NB	NB	NM	Z	Z	PM
	NS	NB	NB	NM	NS	Z	PS	PB
	ZE	NB	NM	NS	Z	PS	PM	PB
	PS	NM	NS	Z	PS	PM	PB	PB
	PM	NM	Z	Z	PM	PB	PB	PB
	PB	NS	Z	Z	PB	PB	PB	PB

The input and output membership functions are shown in figure 18.

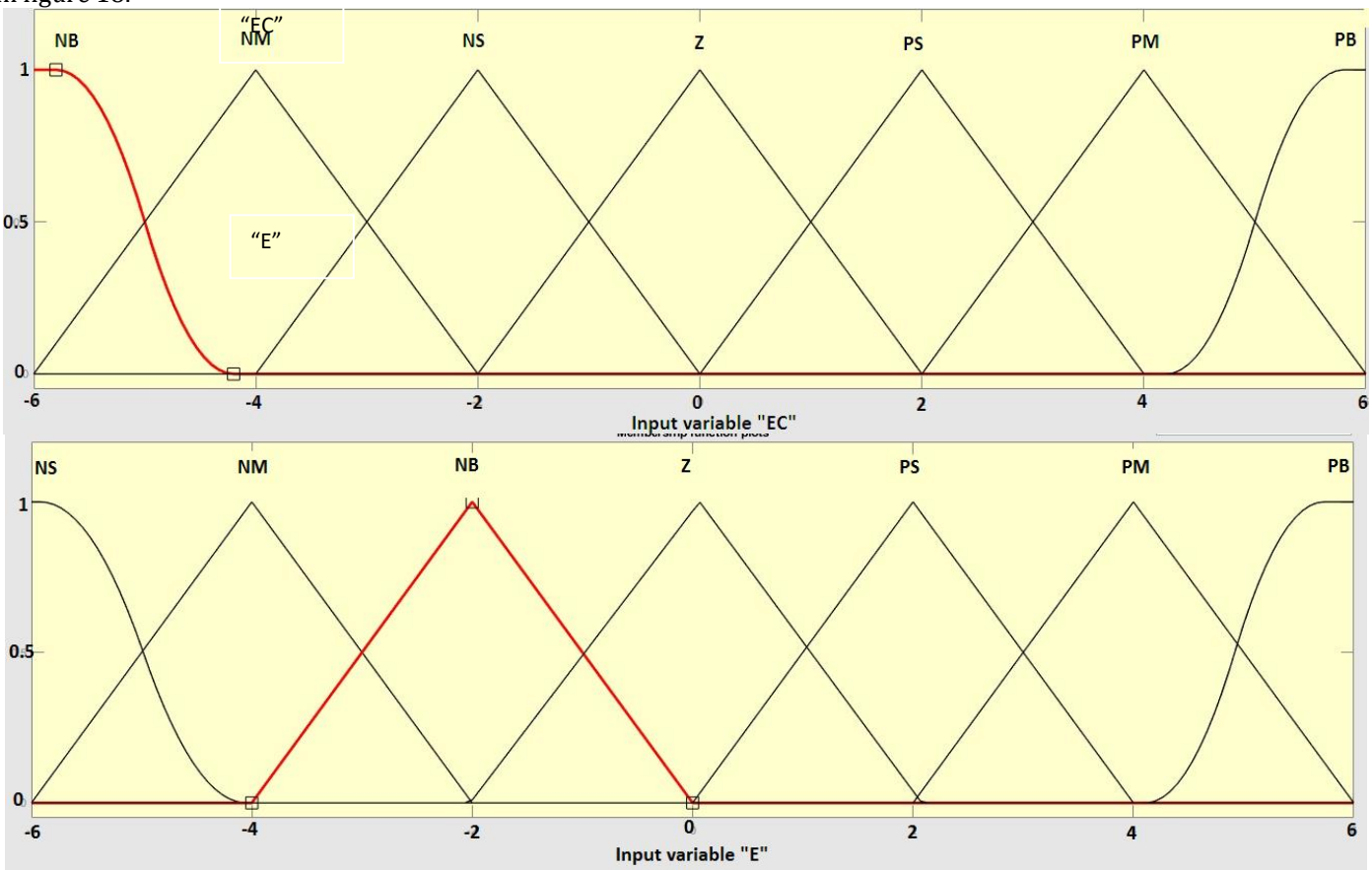

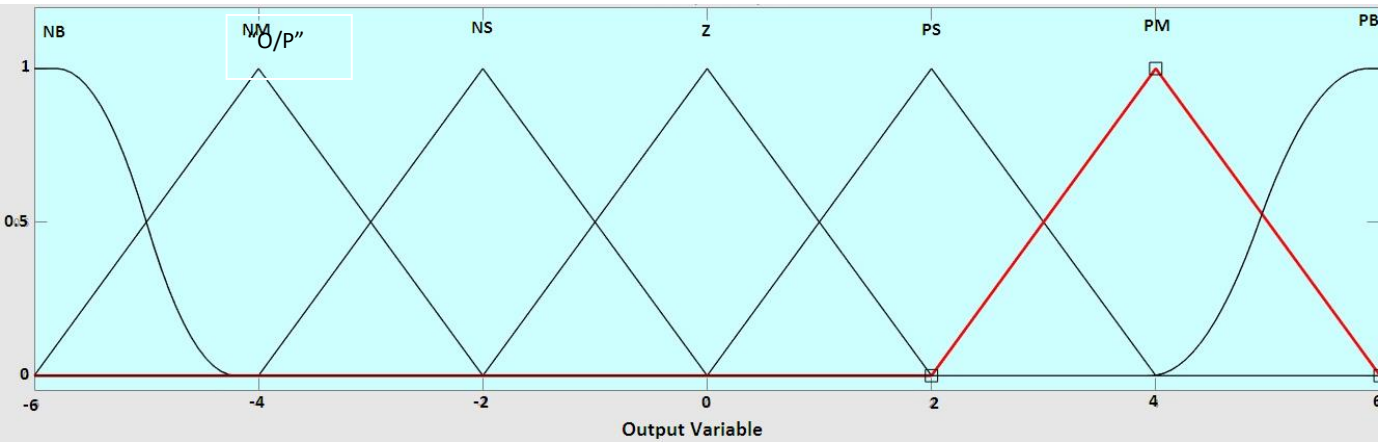

Figure 18. Input (E and EC) and Output Fuzzy membership functions

The input and output fuzzification rule base in graphical form is shown in figure 19.

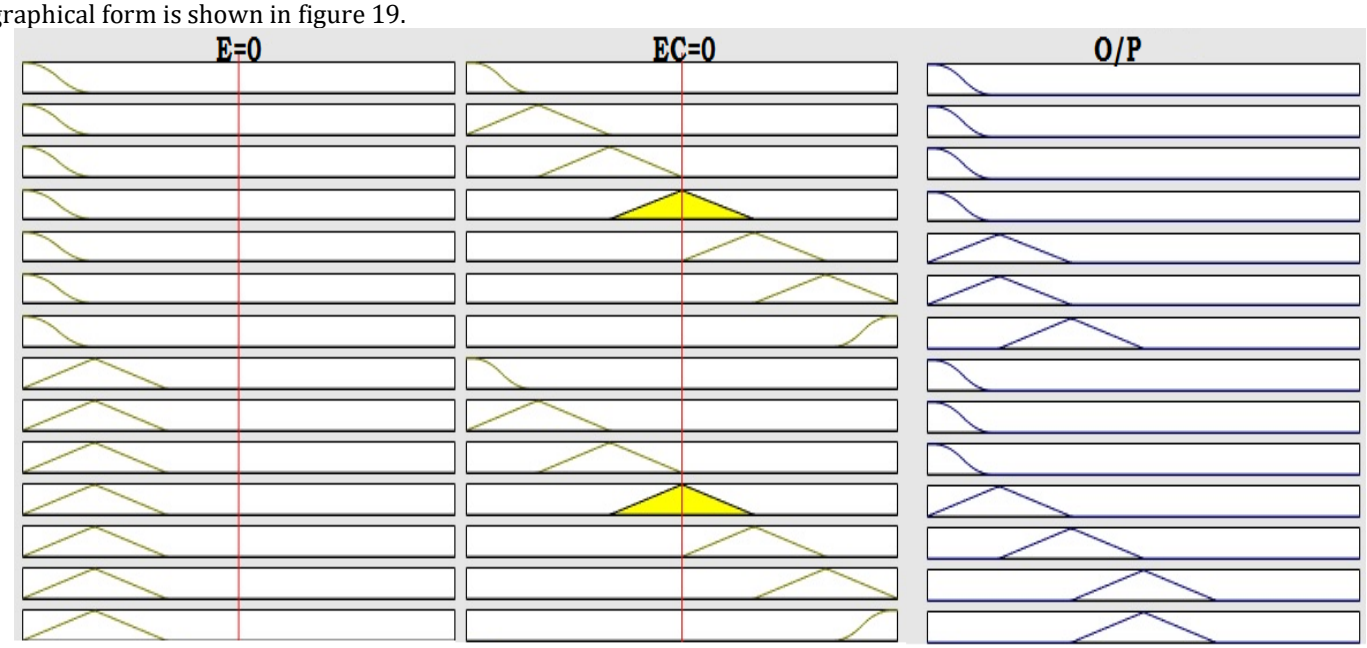

Figure 19. Graphical representation of fuzzy rule base

4. The rule strength and the output membership function are combined together to determine the rule's consequence.

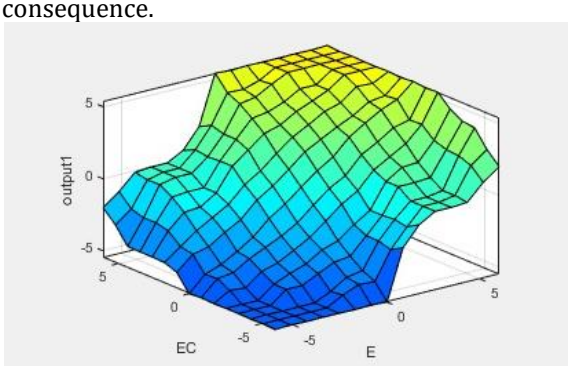

Figure 20. Fuzzy input-output surface viewer

The Surface Viewer of the input variables (E, EC) and the output variable (U) is shown in figure 20.

5. The Rule consequences are combined to get an output distribution and the output is defuzzified using centroid method.

5. Simulation Results

(A) SIMULATION PARAMETERS

In this paper, the controller is developed for a 3-phase 8/6 poles rated 10kW prototype SR motor. The machine parameters are given in Table 2.

Table 2. Machine Design

Parameter	Design data
Power	10 KW
Stator resistance	1.3 ohm
Inertia	0.0013 Kg.m.m
Friction	0.02 N.m.s
Unaligned inductance	1.167e-3H
Aligned inductance	12.87e-3H
Saturated Aligned Inductance	0.625 e-3H
Maximum current	100A
Maximum flux linkage	0.32

(B)SRM WITH SMC CONTROLLER

The starting response of the 8/6 SRM with sliding mode controller is discussed in this section. The starting performance is better with SMC control. However, for change in speed signal or disturbances, the controller overshoot and steady state error is more. The optimization of gain parameters was done and the better results were obtained.

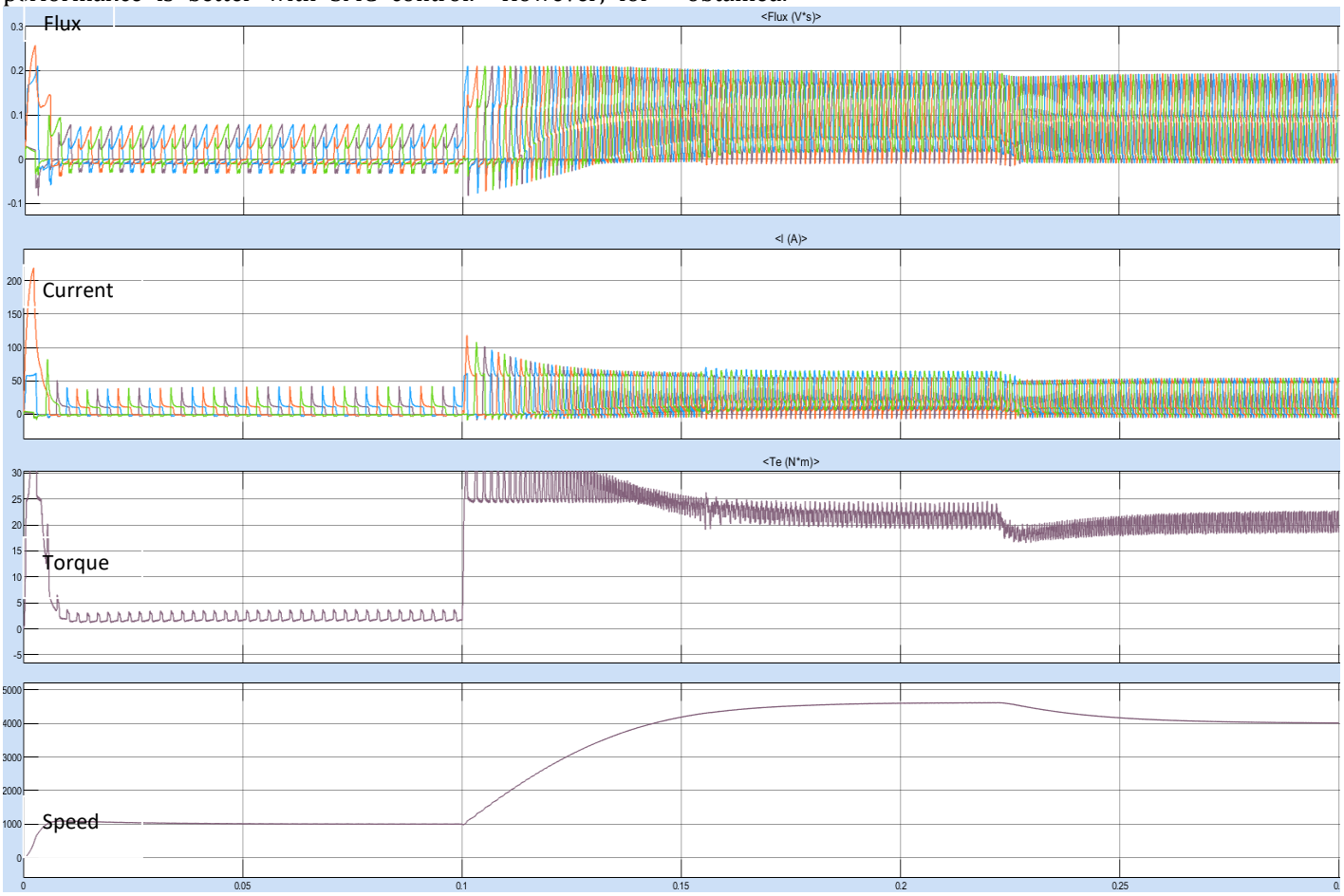

Figure 21. Starting response at 4000rpm with SMC controller

The results of Steady State performance of SRM Drive at 4000RPM is shown in figure 21. The optimal switching angle was iteratively found out through simulation and it was observed, when the switching angle $\boldsymbol{\theta}_{on}$ and $\boldsymbol{\theta}_{off}$ fixed at 30' and 49' respectively, the torque pulsations were minimum.

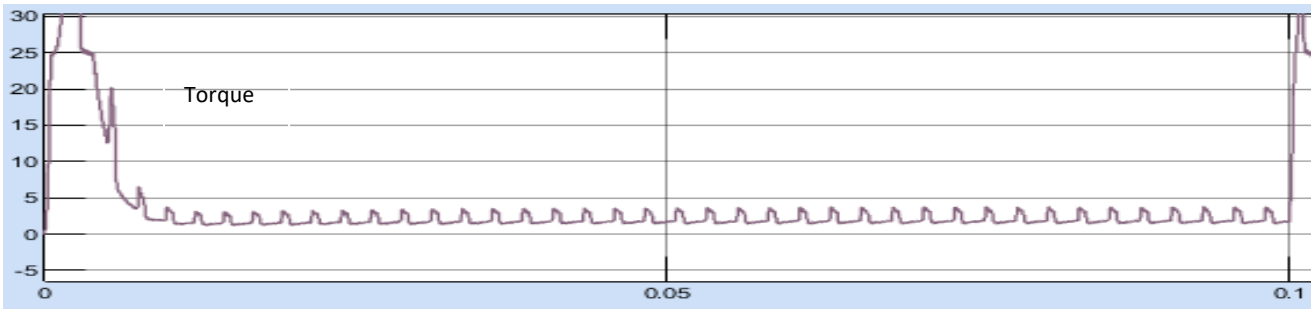

Figure 22. SRM torque at 1000rpm with SMC controller

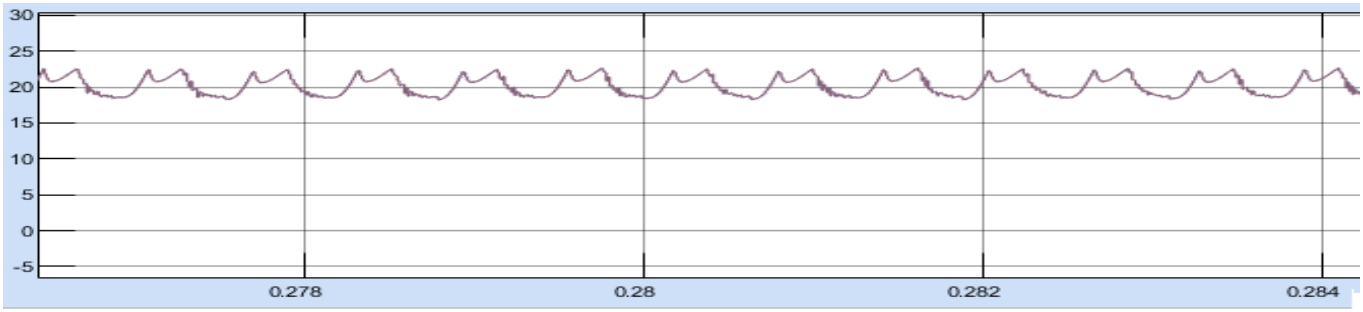

Figure 23. SRM torque at 4000rpm with SMC controller

The torque performance using SMC controller is shown in figure 22 and 23.

Table 3. Torque and torque ripple performance with 1000 and 4000 rpm

Speed	Torque Variation	Ripple
1000 RPM	3-4 Nm	28%
4000 RPM	19-21Nm	19%

The torque ripple is reduced at higher speed is shown in Table 3. The Torque oscillation is observed between 19-21Nm at 4000 rpm. The Torque ripple is 19%.

(C) WITH FUZZY CONTROLLER

For the same machine parameters, the torque performance of 8/6 SRM with Fuzzy logic controller was simulated and The starting response of the 8/6 SRM with FLC is shown in figure 24.

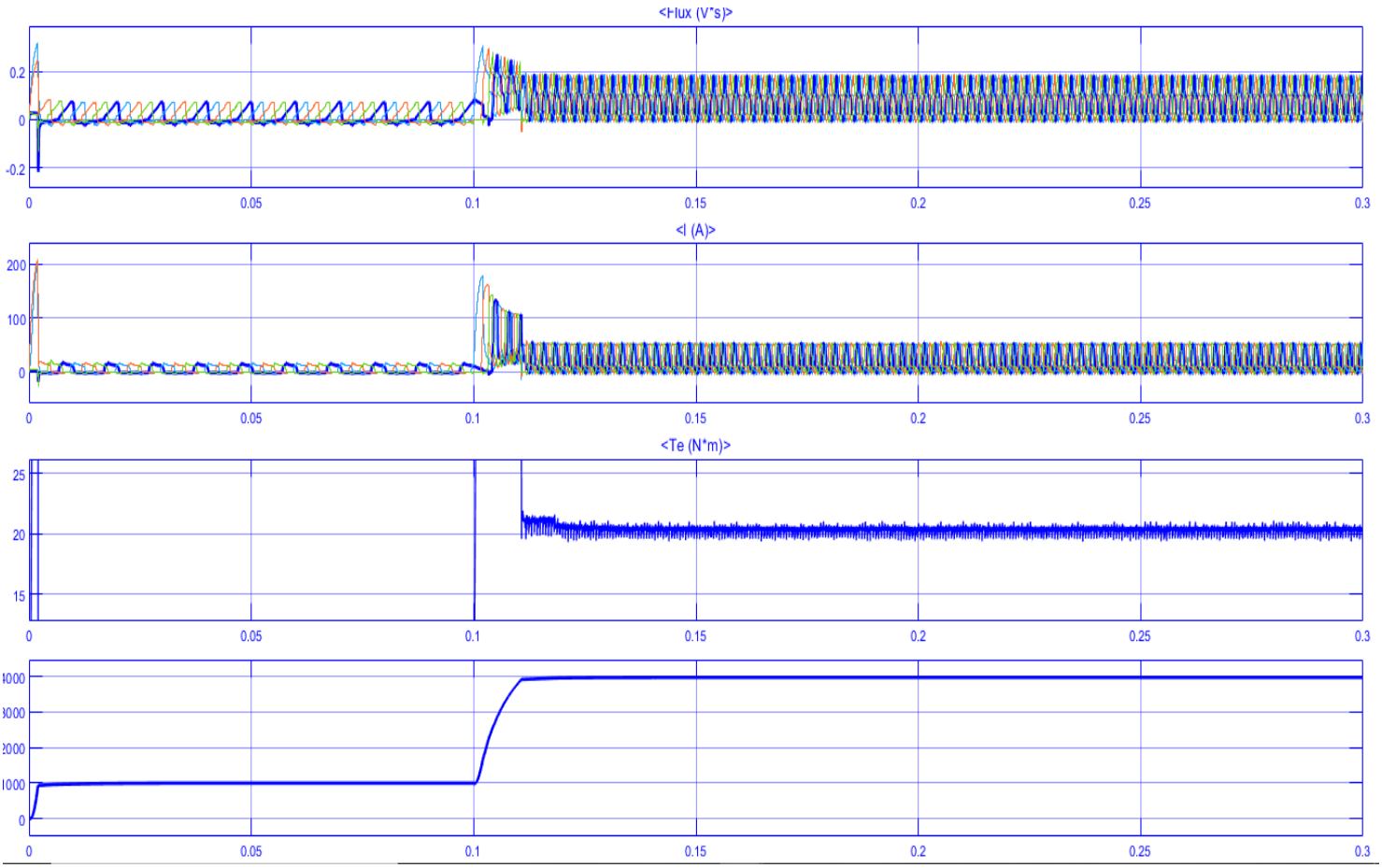

Figure 24. Starting response at 4000rpm with fuzzy controller

The starting response of the motor is very smooth with reduced overshoots and lesser rise time. The steady state error after reaching the stable operating point is also very less. The system is more stable in case of any sudden change in input or any external disturbances. The torque performance of SRM Drive at 4000RPM with fuzzy controller is shown in figure 25.

The Torque oscillation is observed between 19-19.5Nm at 4000 rpm. The Torque ripple is 5%. The torque performance is superior with Fuzzy controller and also the torque ripple is very less compared to Sliding mode controller.

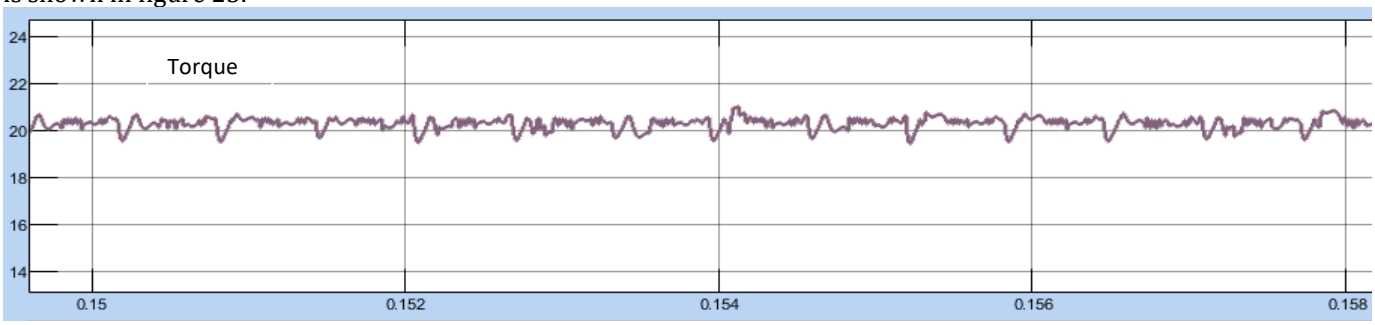

Figure 25. SRM torque at 4000rpm with fuzzy controller

Table 4. Torque and torque ripple performance with 1000 and 4000 rpm

Speed	Torque Variation	Ripple
1000 RPM	3-3.2 Nm	7%
4000 RPM	19.5-20.5Nm	5%

The torque ripple is reduced at higher speed is shown in Table 4. The Torque oscillation is observed between 19-21Nm at 4000 rpm. The Torque ripple is 5%. On comparing table 3 and 4, it is clear that the torque ripple in SRM which is the major limitation for its use in electric vehicle is reduced from 19 % to 5 %.

6. Conclusion

SRM finds itself as a suitable candidate in electric vehicle application. The only limitation is torque ripple, vibration and noise. The torque ripple can be minimized by working on the main dimensions of the machine and also with the converter design. The paper presents the comparison of performance of 8/6 SRM with two different controllers, Sliding mode controller and fuzzy logic controller. Simulation results in mid speed and high speed demonstrate that better torque performance and lesser torque ripple can be achieved with fuzzy controller compared to SMC controller. The torque ripple is reduced by proper gate signal to the converter circuit by governing the excitation to the stator phases. The torque ripple using fuzzy logic controller is found to be 5 % where as using SMC is 19 %. Simulation results show that proposed SRM drive with fuzzy controller decrease steady state errors on any disturbance and also torque ripple, effectively. The method has good performance in wide speed range.

References

1. M. Pittermann, J. Fort, J. Diesl and V. Pavlicek, "Optimal SRM-Control Algorithm to Achieve Maximum Torque and Real Converter Limits," 2018 18th International Conference on Mechatronics - Mechatronika (ME), 2018, pp. 1-8.
2. A. Anand and B. Singh, "Power Factor Correction in Cuk–SEPIC-Based Dual-Output-Converter-Fed SRM Drive," in IEEE Transactions on Industrial Electronics, vol. 65, no. 2, pp. 1117-1127, Feb. 2018, doi: 10.1109/TIE.2017.2733482.
3. S. Shin, N. Kawagoe, T. Kosaka and N. Matsui, "Study on Commutation Control Method for Reducing Noise and Vibration in SRM," in IEEE Transactions on Industry Applications, vol. 54, no. 5, pp. 4415-4424, Sept.-Oct. 2018, doi: 10.1109/TIA.2018.2831173.
4. X. Deng, B. Mecrow, H. Wu and R. Martin, "Design and Development of Low Torque Ripple Variable-Speed Drive System With Six-Phase Switched Reluctance Motors," in IEEE Transactions on Energy Conversion, vol. 33, no. 1, pp. 420-429, March 2018, doi: 10.1109/TEC.2017.2753286.
5. W. Sun, Q. Li, L. Sun, L. Zhu and L. Li, "Electromagnetic Analysis on Novel Rotor-Segmented Axial-Field SRM Based on Dynamic Magnetic Equivalent Circuit," in IEEE Transactions on Magnetics, vol. 55, no. 6, pp. 1-5, June 2019, Art no. 8103105, doi: 10.1109/TMAG.2019.2901002.
6. Y. A. Khan, I. K. Twinkle, S. Kumar and V. Verma, "Comparative Analysis of Different Converter Topologies for an SRM Drive with Conventional and Vector Control Schemes," 2020 International Conference on Emerging Frontiers in Electrical and Electronic Technologies (ICEFEET), 2020, pp. 1-6, doi: 10.1109/ICEFEET49149.2020.9187008.
7. A. Xu, C. Shang, J. Chen, J. Zhu and L. Han, "A New Control Method Based on DTC and MPC to Reduce Torque Ripple in SRM," in IEEE Access, vol. 7, pp. 68584-68593, 2019, doi: 10.1109/ACCESS.2019.2917317.
8. X. Sun, J. Wu, G. Lei, Y. Guo and J. Zhu, "Torque Ripple Reduction of SRM Drive Using Improved Direct Torque Control With Sliding Mode Controller and Observer," in IEEE Transactions on Industrial Electronics, vol. 68, no. 10, pp. 9334-9345, Oct. 2021, doi: 10.1109/TIE.2020.3020026.
9. Z. Wei, M. Zhao, X. Liu and M. Lu, "Speed Control for SRM Drive System Based on Switching Variable Proportional Desaturation PI Regulator," in IEEE Access, vol. 9, pp. 69735-69746, 2021, doi: 10.1109/ACCESS.2021.3078194.
10. Z. Wei, M. Zhao, X. Liu and M. Lu, "Speed Control for SRM Drive System Based on Switching Variable Proportional Desaturation PI Regulator," in IEEE Access, vol. 9, pp. 69735-69746, 2021, doi: 10.1109/ACCESS.2021.3078194.
11. X. Zhang, Q. Yang, M. Ma, Z. Lin and S. Yang, "A Switched Reluctance Motor Torque Ripple Reduction Strategy With Deadbeat Current Control and Active Thermal Management," in IEEE Transactions on Vehicular Technology, vol. 69, no. 1, pp. 317-327, Jan. 2020, doi: 10.1109/TVT.2019.2955218.
12. Q. Sun, J. Wu, C. Gan, J. Si, J. Guo and Y. Hu, "Cascaded Multiport Converter for SRM-Based Hybrid Electrical Vehicle Applications," in IEEE Transactions on Power Electronics, vol. 34, no. 12, pp. 11940-11951, Dec. 2019, doi: 10.1109/TPEL.2019.2909187.
13. K. Aiso and K. Akatsu, "High speed SRM using vector control for electric vehicle," in CES Transactions on Electrical Machines and Systems, vol. 4, no. 1, pp. 61-68, March 2020, doi: 10.30941/CESTEMS.2020.00009.